Atmos. Chem. Phys. Discuss., 14, 18355–18388, 2014
www.atmos-chem-phys-discuss.net/14/18355/2014/
doi:10.5194/acpd-14-18355-2014
© Author(s) 2014. CC Attribution 3.0 License.

Atmospheric Chemistry and Physics Discussions

This discussion paper is/has been under review for the journal Atmospheric Chemistry and Physics (ACP). Please refer to the corresponding final paper in ACP if available.

# Major contribution of neutral clusters to new particle formation in the free troposphere

**C. Rose[1], K. Sellegri[1], E. Asmi[2], M. Hervo[1], E. Freney[1], H. Junninen[3], J. Duplissy[3], M. Sipilä[3], J. Kontkanen[3], K. Lehtipalo[3,4], and M. Kulmala[3]**

[1]Laboratoire de Météorologie Physique CNRS UMR6016, Observatoire de Physique du Globe de Clermont-Ferrand, Université Blaise Pascal, France
[2]Finnish Meteorological Institute, P.O. Box 503, 00101 Helsinki, Finland
[3]Dept. of Physics, University of Helsinki, Helsinki, Finland
[4]Airmodus Ltd, Gutaf Hällströmin katu 2, 00560 Helsinki, Finland

Received: 13 February 2014 – Accepted: 23 June 2014 – Published: 10 July 2014

Correspondence to: K. Sellegri (k.sellegri@opgc.univ-bpclermont.fr)

Published by Copernicus Publications on behalf of the European Geosciences Union.

## Abstract

The formation of new aerosol particles in the atmosphere is a key process influencing the aerosol number concentration as well as the climate, in particular in the free troposphere (FT) where the newly formed particles directly influence cloud formation. However, free tropospheric new particle formation (NPF) is poorly documented due to logistic limitations and complex atmospheric dynamics around high altitude stations that make the observation of this day-time process challenging. Recent improvements in measurement techniques make now possible the detection of neutral clusters down to ∼ 1 nm sizes, which opens new horizons in our understanding of the nucleation process. Indeed, only the charged fraction of clusters has been reported in the upper troposphere up to now. Here we report observations of charged and neutral clusters (1 to 2.5 nm mobility diameter) during day-time free tropospheric conditions at the altitude site of Puy de Dôme (1465 m a.s.l.), central France, between 10 and 29 February 2012. Our findings demonstrate that in the free troposphere, the formation of 1.5 nm neutral clusters is about 40 times higher than the one of ionic clusters during NPF events, indicating that they dominate in the nucleation process. We also observe that the total cluster concentration increases by a factor of 5.5 during NPF events compared to the other days, which was not clearly observed for the charged cluster population in the past. In the FT, the nucleation process does not seem to be sulphuric acid-limited, as previously suggested, and could be promoted by the transport of pollutants to the upper troposphere.

## 1 Introduction

New particle formation directly impacts the total atmospheric aerosol particle concentration and has an indirect effect on climate through cloud related radiative processes (Makkonen et al., 2012). The formation of aerosol particles has been observed and studied in various environments around the world. It appears that depending on the





ACPD
14, 18355–18388, 2014

location, new particle formation (NPF) events do have specificities in term of intensity and space scales, both horizontal (Kulmala et al., 2004) and vertical (Boulon et al., 2011). The formation of new particles in the FT is particularly important as actual global models predict that it contributes to an important fraction of the total atmospheric column aerosol number concentration (Merikanto et al., 2009) and hence potential CCN number concentrations (Spracklen et al., 2008). However, observation of NPF at high altitude is still scarce, especially using the instrumentation adapted to the study of nanometer-sized clusters.

Aerosol formation results from a complex sequence of different processes including the production of clusters from gaseous precursors and the growth of these clusters to particles. Despite the fact that instrumentation is continuously improved, our understanding of the aerosol formation mechanism is still limited. Especially challenging tasks are to quantitatively detect neutral clusters and identify the chemical species involved in the first step of the NPF.

Until a few years ago, the measurement techniques able to detect the smallest cluster sizes were based on electrostatic methods, such as the NAIS (Neutral Air Ion Spectrometer, Mirme and Mirme, 2013). These methods require artificial charging of neutral particles prior to the measurement. Studies concerning the NAIS sampling technique showed that reliable measurements of neutral cluster concentrations could not be ensured for diameters smaller than $\sim 2$ nm because of the post filtering process of corona generated ions (Asmi et al., 2009; Manninen et al., 2011). Recent improvements of condensation techniques make it now possible to measure the concentrations and the size distributions of charged as well as neutral particles down to $\sim 1$ nm sizes (Kim et al., 2003; Vanhanen et al., 2011; Kuang et al., 2012a). This size limit appears to be more relevant for the study of nucleation compared to the 2 nm size limit of the NAIS since it was recently shown that atmospheric nucleation occurs at size $1.5\,\text{nm} \pm 0.4\,\text{nm}$ (Kulmala et al., 2007, 2013; Kirkby et al., 2011). Using PSM (Particle Size Magnifier, Vanhanen et al., 2011) measurements, Kulmala et al. (2013) have recently reported a high variability, both in term of spatial and temporal scales, of neutral cluster concen-





ACPD
14, 18355–18388, 2014

trations at boundary layer sites. In Hyytiälä, Finland, they were also able to quantify the fraction of particles produced exclusively by the neutral pathway, i.e. excluding ion – mediated nucleation and recombination of oppositely charged ions (Kontkanen et al., 2013). Several studies performed prior to the development of the PSM have reported that the charged nucleation pathway seemed to be a more favourable route at high altitude compared to boundary layer (BL) stations for the formation of new particles (Boulon et al., 2010; Manninen et al., 2010).

In this paper, we report the diurnal variability of total, charged and neutral cluster concentrations as well as NPF event characteristics measured between 10 and 29 February 2012 using PSM and NAIS data recorded in clear sky conditions at the Puy de Dôme station (7 days available). This period was selected due to the occurrence of very low temperatures in central and Western Europe, that led to unusually low BL height coupled with increased pollution levels. The low BL height permitted the Puy de Dôme station to lay in the free troposphere (FT) even during day time, when nucleation occurred. Thus, the main purpose of this paper is to investigate cluster formation and concentrations in the FT, with a special focus on neutral clusters.

## 2 Measurements and methods

### 2.1 Measurement site

Measurements were carried out at the Puy de Dôme (PDD) site (45°46′ N, 2°57′ E) in central France (part of European networks EMEP/GAW/ACTRIS). The station is located at the top of the Puy de Dôme mountain (1465 m a.s.l.). and is mainly surrounded by fields and forest. The nearest town, Clermont-Ferrand (300 000 inhabitants), is located 16 km East of the mountain at 396 m a.s.l. More detailed description of the station can be found in Freney et al. (2011).





ACPD
14, 18355–18388, 2014

## 2.2 Instrumentation

### 2.2.1 The Neutral cluster and Air Ion Spetromecter (NAIS)

The charged cluster size distributions were recorded with an NAIS (Airel Ltd., Mirme et al., 2007) which ensures ion measurement in the mobility range 0.0013–3.2 $cm^2\,V^{-1}\,s^{-1}$, corresponding to particle Milikan diameter between 0.8 and 42 nm. The instrument was operating on the roof of the station behind an individual non-heated short inlet (30 cm). This setup implies that measurements are directly influenced by cloudy conditions. The AIS sampling method is based on the simultaneous measurement of positively and negatively charged particles with two identical cylindrical Differential Mobility Analysers (DMA). Each analyser uses a sample flow rate of 30 $L\,min^{-1}$ and a sheath flow rate of 60 $L\,min^{-1}$, which minimizes diffusion losses and ensure significant signal to noise ratio, even in case of low concentrations. The inner cylinder of each DMA is divided into four isolated rings charged with a constant voltage during a measurement cycle. The outer cylinder is made of 21 isolated rings connected to 21 electrometers. Naturally charged aerosol particles are moved in the DMA by a radial electric field from the inner cylinder to the outer one. The current carried by ions entering the DMA is further amplified and measured with electrometers. After a measurement cycle, the instrument runs an offset measurement in order to estimate the noise of the electrometers. During the offset measurement, all the particles, both neutral and charged, must be removed from the sample air before they enter the DMAs. For that purpose, all the particles are thus charged with a unipolar corona charger and electrically filtered before reaching the DMAs.

The NAIS also allows the detection of total particles after a pre-charging process during which particles are charged by ions originating from a corona discharge. The sampling analysis method is then similar to the one described for the ions.





ACPD
14, 18355–18388, 2014

### 2.2.2 The Particle Size Magnifier (PSM)

The total (neutral + ion) cluster concentrations ($N_{tot}$) were measured with a PSM (Airmodus A09, Vanhanen et al., 2011) which allows cluster detection down to ~ 1 nm sizes. The PSM is a mixing-type instrument in which the sampling is based on a rapid and turbulent mixing of aerosol and heated air saturated with diethylene glycol (DEG). Optical particle counting is done with an ordinary CPC (TSI 3010). The sample flow rate of the PSM is fixed at 2.5 L min$^{-1}$ while the saturator flow rate can be varied in the range 0.1–1 L min$^{-1}$, which corresponds to varying the 50 % activation diameter of the instrument between 1–2.5 nm by changing the mixing ratio of the DEG vapor. For the measurements used in this study, the PSM was operating in a scanning mode with 120 steps between saturator flow rates 0.1–1 L min$^{-1}$ and a time resolution of 4 min.

### 2.2.3 Atmospheric pressure Interface time of flight mass spectrometer (APi-TOF)

Chemical composition of atmospheric ions was measured with the APi-TOF, which is described in detail in Junninen et al. (2010). In short, the instrument samples the atmospheric ions at ambient pressure and then transports them through differentially pumped chambers where the ions are focused into an ion beam. The ion beam is diverted onto an orthogonal flight path by an electric field pulse; the time of flight of the ions is determined by the difference between the pulse time and the arrival time at the detector. The flight time of ions is converted to a mass/charge ratio by empirical calibration equations. The small atmospheric ions are all singly charged so by determining the mass/charge ratio, the mass of ions is defined. Mass resolving power of the instrument is about 4000 Th/Th and is defined by Eq. (1):

$$R = \frac{m}{\Delta m} \quad (1)$$

where the $\Delta m$ is width of the peak at half the maximum, and $m$ is the mass.





ACPD
14, 18355–18388, 2014

The high resolution of the APi-TOF makes it possible to define elemental composition for measured ion masses. For example, the resolution $R = 4000\,\mathrm{Th/Th}$ means that at $m = 97\,\mathrm{Th}$, the peak is 0.0243 Th wide (Eq. 1). If at this mass there were a sulphuric acid anion ($HSO_4^-$, $m = 96.9601\,\mathrm{Th}$) and a hypothetical hydrocarbon ($C_7H_{13}^-$, $m = 97.1023\,\mathrm{Th}$), the peaks would be 0.1422 Th apart; that is, 5.8 times the widths of the peak. This example demonstrates how an accurate mass measurement can be used for defining the chemical composition (see details in earlier publications by Junninen et al., 2010; Ehn et al., 2010). In the present study, APi-TOF measurements were not directly used to investigate the cluster composition but rather to modify a proxy for sulfuric acid concentrations at the Puy de Dôme, as explained in Sect. 2.3.1.

### 2.2.4 LIDAR measurements

In order to get an estimation of the boundary layer (BL) height, here assumed to be equal to the aerosol mixing layer height, LIDAR measurements were achieved from the roof of the Laboratoire de Météorologie Physique (45°45′ N, 3°6′ E, 410 m a.s.l.). The LIDAR is a Raymetrics Rayleigh–Mie LIDAR emitting at 335 nm, with both parallel and orthogonal polarization channels. The spatial resolution of the LIDAR is 7.5 m. The instrument provides volume backscatter and extinction profiles, as well as the depolarisation ratio and water vapour mixing ratio. A more complete description of the LIDAR is available in Hervo et al. (2012). The method used for the determination of the BL height is detailed in Sect. 2.3.2.

### 2.2.5 Auxiliary measurements

Auxiliary measurements were used to explain the observed NPF and cluster concentration features reported in the present study. Numerous atmospheric parameters such as global radiation, wind speed and direction, temperature, pressure and relative humidity (RH) as well as atmospheric trace gases (including $SO_2$) and particulate black carbon (BC) are continuously recorded at the station. $SO_2$ measurements were performed





ACPD
14, 18355–18388, 2014

using a low level $SO_2$ analyser (pulsed fluorescence TEI 43CTL) while BC measurements were achieved with a Multi Angle Absorption Photometer (MAAP 5012, central wavelength at 637 nm). The aerosol particle number size distributions were measured with a custom built Scanning Mobility Particle Sizer (SMPS) operating in the size range 10–420 nm. The SMPS, as well as the PSM, were operating behind a Whole Air Inlet (WAI) with a cut-off size of 30 µm. More detailed explanations on the SMPS and the inlet system can be found in Venzac et al. (2009). Since clusters were previously shown to be very sensitive to the presence of clouds at high altitude stations (Lihavainen et al., 2007; Venzac et al., 2007), cloudy conditions were filtered out by using RH data. Indeed, cluster ions, and eventually cluster particles, are very efficiently scavenged by the cloud droplets that offer a large condensational sink. Cluster formation and subsequent growth to larger particle sizes would be difficult to follow due to this very high sink. The threshold value RH = 98 % was used to separate in-cloud and out-of-cloud conditions.

## 2.3 Data analysis

### 2.3.1 Sulphuric acid concentration

Sulphuric acid concentrations ($[H_2SO_4]$) were calculated using a proxy adjusted on concentrations derived from Api-Tof measurements conducted between 30 January and 6 February 2012 at the Puy de Dôme (no data available between 10 and 29 February):

$$[H_2SO_4] = k\frac{\mathrm{GlobRad}\cdot[SO_2]}{\mathrm{CS}\cdot\mathrm{RH}} \quad (2)$$

where $k$ is a scaling factor, and GlobRad is the global radiation in $\mathrm{W\,m^{-2}}$, $[SO_2]$ is the sulphur dioxide concentration in $\mathrm{molec\,cm^{-3}}$, CS is the condensation sink in $\mathrm{s^{-1}}$ and RH is the relative humidity. The form of Eq. (2) was suggested by Mikkonen et al. (2011) and is based on previous work by Petäjä et al. (2009). This proxy was constructed for





ACPD
14, 18355–18388, 2014

radiations higher than 10 W m$^{-2}$ but the predictive ability is significantly raised for radiations exceeding 50 W m$^{-2}$, which was roughly achieved between 7:30 and 16:30 UTC (−1 h LT in winter) during the studied period. As previously mentioned, in the present study, the scaling factor $k = 6.0060 \times 10^{-7}$ cm$^3$ m$^2$ W$^{-1}$ s$^{-1}$ was empirically obtained by using a linear fitting procedure on sulphuric acid concentrations derived from Api-Tof measurements.

### 2.3.2 Boundary layer height determination

The estimation of the BL height was derived from LIDAR data and is based on the fact that aerosol concentrations, and thus the LIDAR signal, show a sudden drop between the BL and the FT. The most common used methods are (1) the measurement of the LIDAR signal variance, (2) the measurement of the LIDAR signal gradient and (3) the analysis of the analogy between the LIDAR signal and a wavelet. The last method, called wavelet covariance technique (WCT), appears to be the most relevant (Baars et al., 2008) and was used in the present study. The WCT uses the covariance transform $W$ of the Haar function $h$ (Brooks, 2003):

$$W(a,b) = \frac{1}{a}\int_{z_b}^{z_t} S(z)h\left(\frac{z-b}{a}\right)\mathrm{d}z \tag{3}$$

with

$$h\left(\frac{z-b}{a}\right) = \begin{cases} 1 & b - \frac{a}{2} \le z \le b \\ -1 & b \le z \le b + \frac{a}{2} \\ 0 & \text{elsewhere} \end{cases} \tag{4}$$

where $z$ is altitude, $S(z)$ is the LIDAR backscatter profile corrected with $z^2$, $z_b$ and $z_t$ are the lower and upper limit of the profile, respectively, $b$ is the altitude at which the





ACPD
14, 18355–18388, 2014

Haar function is centred and $a$ is the spatial extent. $a$ was set to $12\Delta r$ according to Baars et al. (2008), where $\Delta r$ = 7.5 m is the spatial resolution of the LIDAR.

Equation (3) was applied to all LIDAR profiles with a time resolution of 10 min and for each profile the BL height was identified as the maximum of the $W$ function. These calculations were made under the assumptions that (1) topography does not influence the BL height at the location where the LIDAR measurements take place and (2) aerosol particles are homogeneously mixed within the BL. LIDAR measurements were previously used by Boulon et al. (2011) to derive BL height at the Puy de Dôme. In this last study, the reliability of the LIDAR derived BL height was tested and approved using potential equivalent temperature calculations.

### 2.3.3 Particle formation and growth rate calculations

Particle formation and growth rates are key entities to characterize a NPF event, especially in the very first steps of the formation process, i.e. between 1 and 3 nm. As previously mentioned, the PSM was measuring in a scanning mode during the studied period, but the differences between the concentrations of the successive size classes were too small to allow determination of size distributions, and hence any growth rate calculation. Thus we calculated the total particle formation rate at 1.5 nm, $J_{1.5}^{\mathrm{tot}}$, from the total particle concentration measured in the size range 1–2.5 nm by the PSM, $N_{1-2.5}$, and by using the growth rates derived from the NAIS in the ion mode in the size range 1.5–3 nm, $\mathrm{GR}_{1.5-3}$. GRs were calculated with the "maximum concentration" method originating from Hirsikko et al. (2005). In this method, the time corresponding to the maximum concentration in each size class of the selected size range is first determined by fitting a normal distribution to the size class concentration; the growth rate of the corresponding size range is then obtained by a linear least square fit through the time values previously found. The total particle formation rate at 1.5 nm was finally calculated according to Eq. (5), from Kulmala et al. (2007):

$$J_{1.5}^{\mathrm{tot}} = \frac{\mathrm{d}N_{1-2.5}}{\mathrm{d}t} + \mathrm{CoagS}_{1.5} \cdot N_{1-2.5} + \frac{1}{1\,\mathrm{nm}} \mathrm{GR}_{1.5-3} \cdot N_{1-2.5} \quad (5)$$





ACPD
14, 18355–18388, 2014

where $CoagS_{1.5}$ represents the loss of 1.5 nm particles on larger pre-existing particles from the background size distribution. In the case of charged particles, Eq. (5) is completed by two terms to take into account the loss of ions by recombination and the attachment of ions to neutral particles:

$$J^{\pm}_{1.5} = \frac{dN^{\pm}_{1-2.5}}{dt} + CoagS_{1.5} \cdot N^{\pm}_{1-2.5} + \frac{1}{1\,nm} GR_{1.5-3} \cdot N^{\pm}_{1-2.5} + \alpha \cdot N^{\pm}_{1-2.5} N^{\mp}_{<2.5} - \beta \cdot N_{1-2.5} N^{\pm}_{<1} \quad (6)$$

where $N^{\pm}_{1-2.5}$ is the ion number concentration (positive or negative) in diameter range 1–2.5 nm and $N^{\pm}_{<y}$ is the ion concentration below $y$ nm. $\alpha$ and $\beta$ are the ion–ion recombination and the ion–neutral attachment coefficient, respectively, and were assumed to be equal to $1.6 \times 10^{-6}$ cm$^3$ s$^{-1}$ and $0.01 \times 10^{-6}$ cm$^3$ s$^{-1}$, respectively (Tammet and Kulmala, 2005). In order to investigate the evolution of the formation rate as a function of cluster size, similar calculations were done for the formation of 3 nm clusters ($J^{tot}_3$) and ions ($J^{\pm}_3$) by using the cluster concentrations in the size range 3–5 nm and the growth rate over the 3–5 nm diameter range, both derived from NAIS measurements.

## 3 Results and discussion

### 3.1 Charged and neutral cluster concentrations in the free troposphere

#### 3.1.1 Identification of free tropospheric conditions

Between the 10 and the 29 February 2012, seven days were selected because they were characterized by clear skies and they gave a unique chance to investigate free tropospheric conditions during the first part of the day, i.e. when nucleation and early growth of new particles occur. Free tropospheric daytime conditions at the station can only be achieved when convective air mass movements are limited. These conditions were fulfilled during a period of exceptionally cold temperatures during winter 2012 in Europe. Figure 1 shows the BL height derived from LIDAR measurements using the





ACPD
14, 18355–18388, 2014

WCT method (see Sect. 2.3.2). On the 21, 22, 28 and 29, the BL height never exceeds the altitude of the Puy de Dôme, meaning that the station is continuously above the BL. On the contrary, on the 10, 11 and 12, the BL height displays a diurnal variation with a maximum between 1700 and 2000 m a.s.l. around 17:00 UTC (−1 h LT in winter). During these days, the Puy de Dôme is in the FT until 12:00 UTC and is progressively reached by the BL in the afternoon. During these free tropospheric conditions, five days were classified as NPF event days (10, 11, 12, 28 and 29 February) based on a visual analysis of the contour plot of the ion size distribution. The remaining two days (21 and 22 February) were considered as non-event days.

Previous observations of cluster and aerosol size distributions at high altitudes have rarely shown NPF events unambiguously occurring in the FT. NPF events at high altitudes were always observed to occur during upwind valley winds (Venzac et al., 2008), or very close to the interface between the BL and the FT (Boulon et al., 2011). The present observations are hence one of the first showing NPF in the FT during clear sky conditions.

### 3.1.2 Charged and neutral cluster concentrations

We measured total ($N_{tot}$) and charged ($N_i$) cluster concentrations in the range 1–2.5 nm mobility diameter, using respectively the PSM and the NAIS. The neutral cluster concentrations ($N_n$) in the same size range were calculated according to $N_n = N_{tot} - N_i$. In agreement with previous observations at the site (Manninen et al., 2009; Boulon et al., 2011; Rose et al., 2013) cluster ions appear to be present on both event and non-event days. Charged cluster concentrations do not show any clear diurnal variations and are on average decreased by a factor 1.5 on event days, being $399 \pm 234\ cm^{-3}$ compared to $556 \pm 101\ cm^{-3}$ on non-event days (Fig. 2). Positive cluster ion concentrations always exceed negative cluster concentrations, by a factor of 2.7 on event days and 3.6 on non-event days. These observations contrast with the general behaviour of positive ions concentration previously observed by Rose et al. (2013), who reported that positive cluster ions concentrations were increased during NPF events over a five years





ACPD
14, 18355–18388, 2014

long study. Especially in winter, the average positive cluster ion concentrations were reported to increase by a factor of 1.24–1.92 on event days compared to non-event days during the time period 10:00–16:00 (UTC). This particular behaviour of positive ions might be explained by the exceptional atmospheric conditions – especially low temperatures and free tropospheric conditions – observed in February 2012 (Fig. 4a).

In contrast with the behaviour of cluster ions, the total cluster concentration displays very different trends and values on event days compared to non-event days (Fig. 2). On non-event days, the total cluster concentration does not significantly vary with the time of the day and is almost continuously below the cluster ion concentration. This last observation supports the fact that the PSM could be unable to detect all of the cluster ions, most likely because of their chemical composition (Kangasluoma et al., 2013; Wimmer et al., 2013). In the present study, we observed that for ion concentrations below $\sim 500\,\mathrm{cm}^{-3}$, the total cluster concentration measured by the PSM was systematically lower than the ion concentration, leading to non-physical negative values for the neutral cluster concentration. In order to remain physically correct, we decided to introduce a lower detection limit (LDL) of $500\,\mathrm{cm}^{-3}$ for total cluster concentrations at and to filter out all the total cluster concentrations that were below this limit. Hence, the total cluster concentrations that we report in this work are a lower limit of the actual total cluster concentrations.

On event days, the total cluster concentration exhibits a very clear diurnal variation with a maximum detected between 10:30 and 14:00 UTC. One should note that these maximum significantly vary from day to day, with values up to $18\,280\,\mathrm{cm}^{-3}$ on the 10 February, which contrast with the maximum detected on the 28 which does not exceed $1524\,\mathrm{cm}^{-3}$. This diurnal variation can be explained by the formation of clusters during the nucleation process in the morning and their growth and/or removal on pre-existing particles in the afternoon. During the nucleation hours (10:30–14:00 UTC), the total cluster concentration is in the range $3345 \pm 3590\,\mathrm{cm}^{-3}$ and more frequently exceeds the charged cluster concentration ($495 \pm 140\,\mathrm{cm}^{-3}$). Especially, averaged neutral cluster concentrations exceed the charged cluster concentration by a factor 6.2 and the





ACPD
14, 18355–18388, 2014

charged fraction $f = N_i/N_{tot}$ is close to 0.3 during the nucleation peak. Outside of the nucleation hours, total cluster concentrations are below the charged cluster concentration, being very similar to the concentrations recorded on non-event days.

The continuous presence of cluster ions has already been reported by several studies at BL stations (Manninen et al., 2009) and at high altitude sites (Boulon et al., 2010; Rose et al., 2013), as well as the diurnal variation of the charged cluster concentration on event days (Hõrrak et al., 2008; Boulon et al., 2010; Rose et al., 2013). According to recent studies, the neutral clusters also seem to be ubiquitous in the atmosphere (Lehtipalo et al., 2009, 2010). In their paper, Kulmala et al. (2013) reported a continuous presence of sub-2.1 nm neutral clusters in Hyytiälä, Finland, with concentrations in the range 500–20 000 $cm^{-3}$. In Finokalia, Greece, sub-2.5 nm total cluster concentrations were in the range 10–10 000 $cm^{-3}$, with lower values at night.

The first observations reported in this section suggest that at the Puy de Dôme, differences between the charged and total cluster concentrations are significant enough to conclude that during free tropospheric conditions, the formation of neutral clusters dominates the formation of total clusters during NPF events. A detailed analysis of the particle formation and growth rates is shown in the following section.

### 3.1.3 Particle formation and growth rates

Figure 3 shows the average diurnal variation of the total and charged formation rates at 1.5 and 3 nm during day time on NPF event days. More information concerning NPF event characteristics is given in Table 1 for each event day. The average formation rates of neutral 1.5 nm particles exceed those of charged particles by a factor of 40 on event days. Charged formation rates of positive 1.5 nm clusters are significantly higher than the charged formation rates of negative 1.5 nm clusters. Similar observations were reported in the CLOUD (Cosmics Leaving Outdoor Droplets) experiment (Kirkby et al., 2011), which studied the role of sulphuric acid, ammonia and ions in the nucleation process. In particular, the occurrence of ternary nucleation involving sulphuric acid and





ACPD
14, 18355–18388, 2014

ammonia with typical path on positive way could explain the excess of positive ions, at least on event days.

In can be seen from Fig. 3 and Table 1 that the formation rates of charged and neutral 3 nm particles are significantly decreased compared to the formation rates of charged and neutral 1.5 nm clusters, which is due to the loss of small particles by coagulation on bigger pre-existing particles during their growth.

The different formation rates exhibit significant variations with the time of the day, and especially $J_{1.5}^{tot}$ with maximum averaged values close to 7.7 $cm^{-3}$ $s^{-1}$ obtained between 11:00 and 15:00, which are almost 40 times higher than the minimum values at 8:00 UTC (Fig. 3). Differences are also observable when comparing one day to another: again $J_{1.5}^{tot}$ shows the most extreme values, with a maximum to minimum ratio of 43 (Table 1).

GR values also experience significant variations between the different events, with a maximum to minimum ratio of 8.7 for $GR_{1.5–3}$ and 4.3 for $GR_{3–5}$. Particularly, on the 12 and the 29, which correspond to the strongest particle formation events, $GR_{1.5–3}$ displays values larger than 10 nm $h^{-1}$. In contrast with the particle formation rate, the particle growth rate is on average increasing as function of particle size in free tropospheric conditions at the Puy de Dôme (Table 1), suggesting the participation of other vapours than sulphuric acid (Kuang et al., 2012b; Kulmala et al., 2013).

The results we obtain clearly suggest that in free tropospheric conditions, the formation of neutral clusters dominates the formation of total clusters during NPF events. This observation goes in the same direction as Lehtipalo et al. (2010) and Kulmala et al. (2013) who observed a very small contribution of ions in the dynamics of sub-2 nm clusters during the nucleation process at the BL site of Hyytiälä. Indeed, both the concentrations of sub-2 nm clusters and the formation rate of 1.5 nm clusters were found to be clearly dominated by neutral particles, sometimes with differences exceeding several orders of magnitude. $J_{1.5}^{tot}$ values reported for Hyytiälä are similar to the values obtained at the Puy de Dôme, with maximum values around 5 $cm^{-3}$ $s^{-1}$ at 12:00 UTC. On the contrary, $J_{1.5}^{\pm}$ exhibits slightly lower values in Hyytiälä, being in the





ACPD
14, 18355–18388, 2014

range $3 \times 10^{-2}$–$6 \times 10^{-2}$ $cm^{-3}$ $s^{-1}$. This observation is in agreement with the previous observations by Boulon et al. (2010) and Manninen et al. (2010) who suggested that charged nucleation pathways could be promoted at higher altitudes compared to low altitudes.

The purpose of the following section is now to investigate the atmospheric conditions that could favor NPF in the FT at the Puy de Dôme and their link to neutral cluster concentrations.

### 3.2 Analysis of the atmospheric conditions promoting particle formation in the free troposphere – evidence for a free troposphere feeding process

As previously mentioned, among the seven studied days, five were identified as event days and the remaining two as non-event days. We further investigated the changes in the free tropospheric conditions which lead or not to NPF during this period. For this purpose, the entire dataset was divided into 3 sub-periods according to the observed atmospheric parameters, including temperature, relative humidity, black carbon concentrations, BL height and three days air mass back trajectories (calculated from the HYSPLIT transport and dispersion mode, Draxler and Rolph, 2003), as well as condensation sink (CS) and sulphuric acid concentration ($[H_2SO_4]$). Overviews of cluster concentrations and atmospheric parameters during the 3 sub-periods are given in Fig. 4 and Tables 2 and 3.

#### 3.2.1 Description of the atmospheric conditions in each sub-period

The first sub-period, referred as "Period 1", includes the 10, 11 and 12 February, during which the Puy de Dôme was not completely disconnected from the BL outside nucleation hours (Fig. 1). Consequently, Period 1 is characterized by high RH (on average 90.8 %) (Fig. 4b and Table 3) and displays the highest BC concentrations, with maximum values up to 1860 $ng\,m^{-3}$ (Fig. 4c). This relatively high level of pollution for the site is also explained by air masses coming from Eastern Europe, especially on the





ACPD
14, 18355–18388, 2014

11 (Fig. 5). High emissions can originate from biomass and fuel burning from intensive domestic heating due to very cold temperatures occurring during this period, which never exceed −12 °C at the Puy de Dôme, being on average −14.2 °C (Fig. 4a). The condensation sink is logically well correlated with BC concentrations and displays the highest average value ($1.36 \times 10^{-2}\,s^{-1}$) of the three sub-periods (Fig. 4d). On the contrary, sulphuric acid concentrations are the lowest of the entire measurement period, with an average value of $6.984 \times 10^{6}$ molec cm$^{-3}$ (Fig. 4e).

The second sub-period, referred as "Period 2", includes the 21 and 22 February. During these two days, the BL height rarely reaches the altitude of the station, suggesting that the Puy de Dôme is hardly influenced by BL direct emissions (Fig. 1). As a consequence, RH and BC concentrations are significantly decreased compared to Period 1, with average values of 29.3 % for RH and typical values in the range 70–420 ng m$^{-3}$ for BC (Fig. 4b and c). Beside the lower altitude of the BL height relative to the site, these lower concentrations may be partly attributed to the geographical origin of air masses reaching the Puy de Dôme that have turned from Northern Europe sector (Fig. 5), and which have already been reported to be less polluted than Eastern air masses (Venzac et al., 2009; Bourcier et al., 2012). At last, temperatures are higher during Period 2 compared to Period 1 (Fig. 4a), which may also lead to less domestic heating and thus lower pollution originating from combustion processes. Consequently, we observe that the condensation sink is also decreased and displays the lowest values of the whole studied period, being on average $1.60 \times 10^{-3}\,s^{-1}$ (Fig. 4d). At the same time, sulphuric acid concentrations are increased compared to Period 1, being the highest of the three sub-periods (Fig. 4e).

The last period, referred as "Period 3", includes the 28 and 29 February. Period 3 is characterized by the same BL heights as Period 2 (Fig. 1) but both RH and CS (no information concerning BC concentrations because of instrument failure) are slightly higher than during Period 2, with average values of 51.8 % and $2.4 \times 10^{-3}\,s^{-1}$, respectively (Fig. 4b and d). Nonetheless, it is worth to note that they remain broadly lower than during Period 1. During Period 3 temperatures continue to increase, so that the





ACPD
14, 18355–18388, 2014

contribution of combustion sources to the condensation sink is likely further decreased (Fig. 4a). However, during Period 3, air masses originate from the north-east part of Europe and they cross UK Islands before reaching the Puy de Dôme (Fig. 5). Thus they are more polluted than the air masses arriving during Period 2. Sulphuric acid concentrations appear to be significantly lower than during Period 2, with an average value of $8.59 \times 10^6$ molec cm$^{-3}$ (Fig. 4e).

### 3.2.2 The role of sulphuric acid

Based on Fig. 4, Tables 1 and 3, we can first assert that $H_2SO_4$ is not the main driver of the nucleation process at the Puy de Dôme in the FT. Indeed, despite the fact that Period 2 is characterized by the highest sulphuric acid concentrations, no NPF events were detected during these days. It is worth to note that similar conclusions are obtained when using proxies for the sulphuric acid concentration that includes scaling factors from the literature, such as the ones proposed in Petäjä et al. (2009) or Mikkonen et al. (2011).

Also, there is no clear correlation between cluster concentrations and sulphuric acid, as illustrated by Fig. 6a. This observation supports the analysis of Boulon et al. (2010, 2011) who reported that at high altitude stations such as the Puy de Dôme and the Jungfraujoch, Switzerland, gaseous precursors other than sulphuric acid were also involved in the formation and early growth of the clusters into new particles.

### 3.2.3 The free troposphere feeding process

The second important result highlighted by Tables 1–3 and Fig. 6b is that both the occurrence of NPF and neutral cluster concentrations are not anti-correlated with the condensation sink. This is clearly visible for Period 1, which displays CS values with one order of magnitude higher than Period 2 and 3 and neutral cluster concentrations increased by a factor closed to 7 compared to Period 3. This observation contradicts the previous result by Boulon et al. (2011) at the Puy de Dôme for ionic clusters but





ACPD
14, 18355–18388, 2014

supports the results reported at the Jungfraujoch station (Boulon et al., 2010). In the present study it is likely that condensable compounds involved in the NPF process and condensation sink share the same origin. Gaseous precursors other than sulphuric acid could be oxidized volatile organic compounds, as suggested by several studies (Metzger et al., 2010; Paasonen et al., 2010; Wang and Wexler, 2013). This would explain the fact that during Period 2, which is characterized by the lowest condensation sinks, particle formation is not triggered because of a lack of other gaseous precursors. Thus, our observations suggest that particle formation occurs when the pool of gaseous precursors is supplied to the FT by inputs of polluted air masses. Similar observations were reported by Neitola et al. (2011) at a high altitude Indian Himalayan site (2180 m a.s.l.). Such a process could be assimilated to a "free troposphere feeding" process.

## 4 Conclusion

We investigated the contributions of total, charged and neutral cluster concentrations (1–2.5 nm) during NPF events observed to occur above the BL at the Puy de Dôme station, during a period characterized by very low temperatures in Europe.

Clusters ions were always present and their concentrations did not exhibit any clear diurnal variation, with slightly higher concentrations on non-event days compared to event days. On the contrary, on event days, the total cluster concentrations clearly peaked between 10:30 and 14:00 (UTC), with concentrations in the range $3345 \pm 3590\,\mathrm{cm}^{-3}$. This is mainly due to increased neutral cluster concentrations which display high maximum on event days on the same time period, and lead to charged fraction down to 0.3.

Total and charged formation rates at 1.5 nm ($J_{1.5}^{\mathrm{tot}}$ and $J_{1.5}^{\pm}$ respectively) were derived from PSM and NAIS respectively. Contrary to $J_{1.5}^{\pm}$, total formation rates displayed a diurnal variation with maximum values up to $7.7\,\mathrm{cm}^{-3}$ obtained between 11:00 and 15:00 UTC on event days. $J_{1.5}^{\mathrm{tot}}$ was on average 40 times higher than $J_{1.5}^{\pm}$, suggesting





ACPD
14, 18355–18388, 2014

that neutral clusters were clearly driving the first steps of the NPF process at the Puy de Dôme.

When investigating the atmospheric conditions promoting nucleation in the FT, we found that sulphuric acid was not the main species driving the nucleation and early growth process since there was no clear link between sulphuric acid and the cluster concentrations, nor between sulphuric acid and the occurrence of NPF. The increasing growth rate of clusters with size support the observation of sulphuric acid not being the only contributor to early particle growth. At last, NPF events were detected when the highest condensation sinks were obtained, suggesting that gaseous precursors other than sulphuric acid could share the same origin as the condensation sink. According to our observations, it is likely that in the free troposphere, particle formation occurs when the amount of gaseous precursors available for nucleation is supplied by inputs of polluted air masses from the BL in a "free troposphere feeding" process.

*Acknowledgements.* Support was provided by AXA, Actris, ACI-AMS, the Academy of Finland Center of Excellence program (project no. 1118615), ERC-Advanced "ATMNUCLE" grant no. 227463), CRAICC and the Nordic Center of Excellence CRAICC.

## References

Asmi, E., Sipilä, M., Manninen, H. E., Vanhanen, J., Lehtipalo, K., Gagné, S., Neitola, K., Mirme, A., Mirme, S., Tamm, E., Uin, J., Komsaare, K., Attoui, M., and Kulmala, M.: Results of the first air ion spectrometer calibration and intercomparison workshop, Atmos. Chem. Phys., 9, 141–154, doi:10.5194/acp-9-141-2009, 2009.

Baars, H., Ansmann, A., Engelmann, R., and Althausen, D.: Continuous monitoring of the boundary-layer top with lidar, Atmos. Chem. Phys., 8, 7281–7296, doi:10.5194/acp-8-7281-2008, 2008.

Boulon, J., Sellegri, K., Venzac, H., Picard, D., Weingartner, E., Wehrle, G., Collaud Coen, M., Bütikofer, R., Flückiger, E., Baltensperger, U., and Laj, P.: New particle formation and ultrafine charged aerosol climatology at a high altitude site in the Alps (Jungfraujoch, 3580 m a.s.l., Switzerland), Atmos. Chem. Phys., 10, 9333–9349, doi:10.5194/acp-10-9333-2010, 2010.





ACPD
14, 18355–18388, 2014

Boulon, J., Sellegri, K., Hervo, M., Picard, D., Pichon, J.-M., Fréville, P., and Laj, P.: Investigation of nucleation events vertical extent: a long term study at two different altitude sites, Atmos. Chem. Phys., 11, 5625–5639, doi:10.5194/acp-11-5625-2011, 2011.

Bourcier, L., Sellegri, K., Chausse, P., Pichon, J. M., and Laj, P.: Seasonal variation of water-soluble inorganic components in aerosol size-segregated at the Puy de Dôme station (1,465 m a.s.l.), France, J. Atmos. Chem., 69, 47–66, doi:10.1007/s10874-012-9229-2, 2012.

Brooks, I. M.: Finding boundary layer top: application of a wavelet covariance transform to lidar backscatter profiles, J. Atmos. Ocean. Tech., 20, 1092–1105, doi:10.1175/1520-0426(2003)020<1092:FBLTAO>2.0.CO;2, 2003.

Draxler, R. R. and Rolph, G. D.: HYSPLIT (Hybrid Single-Particle Langrangian Integrated Trajectory) Model access via NOAA ARL READY website, available at: http://www.arl.noaa.gov/ready/hysplit4.html (last access: 4 July 2014), 2003.

Ehn, M., Junninen, H., Petäjä, T., Kurtén, T., Kerminen, V.-M., Schobesberger, S., Manninen, H. E., Ortega, I. K., Vehkamäki, H., Kulmala, M., and Worsnop, D. R.: Composition and temporal behavior of ambient ions in the boreal forest, Atmos. Chem. Phys., 10, 8513–8530, doi:10.5194/acp-10-8513-2010, 2010.

Freney, E. J., Sellegri, K., Canonaco, F., Boulon, J., Hervo, M., Weigel, R., Pichon, J. M., Colomb, A., Prévôt, A. S. H., and Laj, P.: Seasonal variations in aerosol particle composition at the puy-de-Dôme research station in France, Atmos. Chem. Phys., 11, 13047–13059, doi:10.5194/acp-11-13047-2011, 2011.

Hirsikko, A., Laakso, L., Horrak, U., Aalto, P. P., Kerminen, V., and Kulmala, M.: Annual and size dependent variation of growth rates and ion concentrations in boreal forest, Boreal Environ. Res., 10, 357–369, 2005.

Hõrrak, U., Aalto, P. P., Salm, J., Komsaare, K., Tammet, H., Mäkelä, J. M., Laakso, L., and Kulmala, M.: Variation and balance of positive air ion concentrations in a boreal forest, Atmos. Chem. Phys., 8, 655–675, doi:10.5194/acp-8-655-2008, 2008.

Junninen, H., Ehn, M., Petäjä, T., Luosujärvi, L., Kotiaho, T., Kostiainen, R., Rohner, U., Gonin, M., Fuhrer, K., Kulmala, M., and Worsnop, D. R.: A high-resolution mass spectrometer to measure atmospheric ion composition, Atmos. Meas. Tech., 3, 1039–1053, doi:10.5194/amt-3-1039-2010, 2010.

Kangasluoma, J., Junninen, H., Lehtipalo, K., Mikkilä, J., Vanhanen, J., Attoui, M., Sipilä, M., Worsnop, D., Kulmala, M., and Petäjä, T.: Remarks on ion generation for CPC





ACPD
14, 18355–18388, 2014

detection efficiency studies in sub-3-nm size range, Aerosol Sci. Tech., 47, 556–563, doi:10.1080/02786826.2013.773393, 2013.
Kim, C. S., Okuyama, K., and De la Mora, J. F.: Performance evaluation of an improved particle size magnifier (PSM) for single nanoparticle detection, Aerosol Sci. Tech., 37, 791–803, 2003.
Kirkby, J., Curtius, J., Almeida, J., Dunne, E., Duplissy, J., Ehrhart, S., Franchin, A., Gagné, S., Ickes, L., Kürten, A., Kupc, A., Metzger, A., Riccobono, F., Rondo, L., Schobesberger, S., Tsagkogeorgas, G., Wimmer, D., Amorim, A., Bianchi, F., Breitenlechner, M., David, A., Dommen, J., Downard, A., Ehn, M., Flagan, R.C., Haider, S., Hansel, A., Hauser, D., Jud, W., Junninen, H., Kreissi, F., Kvashin, A., Laaksonen, A., Lehtipalo, K., Lima, J., Lovejoy, E.R., Makhmutov, V., Mathot, S., Mikkilä, J., Minginette, P., Mogo, S., Nieminen, T., Onnela, A., Pereira, P., Petäjä, T., Schnitzhofer, R., Seinfield, J. H., Sipilä, M., Stozhkov, Y., Stratmann, F., Tomé, A., Vanhanen, J., Viisanen, Y., Vrtala, A., Wagner, P. E., Walther, H., Weingartner, E., Wex, H., Winkler, P. M., Carslaw, K. S., Worsnop, D. R., Baltensperger, and Kulmala, M.: Role of sulphuric acid, ammonia and galactic cosmic rays in atmospheric aerosol nucleation, Nature, 476, 429–433, doi:10.1038/nature10343, 2011.
Kontkanen, J., Lehtinen, K. E. J., Nieminen, T., Manninen, H. E., Lehtipalo, K., Kerminen, V.-M., and Kulmala, M.: Estimating the contribution of ion–ion recombination to sub-2 nm cluster concentrations from atmospheric measurements, Atmos. Chem. Phys., 13, 11391–11401, doi:10.5194/acp-13-11391-2013, 2013.
Kuang, C., Chen, M., McMurry, P. H., and Wang, J.: Modification of laminar flow ultrafine condensation particle counters for the enhanced detection of 1 nm condensation nuclei, Aerosol Sci. Tech., 46, 309–315, 2012a.
Kuang, C., Chen, M., Zhao, J., Smith, J., McMurry, P. H., and Wang, J.: Size and time-resolved growth rate measurements of 1 to 5 nm freshly formed atmospheric nuclei, Atmos. Chem. Phys., 12, 3573–3589, doi:10.5194/acp-12-3573-2012, 2012b.
Kulmala, M., Vehkamäki, H., Petäjä, T., Dal Maso, M., Lauri, A., Kerminen, V.-M., Birmili, W., and McMurry, P. H.: Formation and growth rates of ultrafine atmospheric particles: a review of observations, J. Aerosol Sci., 35, 143–176, 2004.
Kulmala, M., Riipinen, I., Sipilä, M., Manninen, H. E., Petäjä, T., Junninen, H., Maso, M. D., Mordas, G., Mirme, A., Vana, M., Hirsikko, A., Laakso, L., Harrison, R. M., Hanson, I., Leung, C., Lehtinen, K. E. J., and Kerminen, V.-M.: Toward direct measurement of atmospheric nucleation, Science, 318, 89–92, doi:10.1126/science.1144124, 2007.





ACPD
14, 18355–18388, 2014

Kulmala, M., Kontkanen, J., Junninen, H., Lehtipalo, K., Manninen, H. E., Nieminen, T., Petäjä, T., Sipilä, M., Schobesberger, S., Rantala, P., Franchin, A., Jokinen, T., Järvinen, E., Äijälä, M., Kangasluoma, J., Hakala, J., Aalto, P. P., Paasonen, P., Mikkilä, J., Vanhanen, J., Aalto, J., Hakola, H., Makkonen, U., Ruuskanen, T., Mauldin III., R. L., Duplissy, J., Vehkamäki, H., Bäck, J., Kortelainen, A., Riipinen, I., Kurtén, T., Johnston, M. V., Smith, J. N., Ehn, M., Mentel, T. F., Lehtinen, K. E. J., Laaksonen, A., Kerminen, V.-M., and Worsnop, D. R.: Direct observations of atmospheric aerosol nucleation, Science, 339, 943–946, doi:10.1126/science.1227385, 2013.

Lehtipalo, K., Sipilä, M., Riipinen, I., Nieminen, T., and Kulmala, M.: Analysis of atmospheric neutral and charged molecular clusters in boreal forest using pulse-height CPC, Atmos. Chem. Phys., 9, 4177–4184, doi:10.5194/acp-9-4177-2009, 2009.

Lehtipalo, K., Kulmala, M., Sipilä, M., Petäjä, T., Vana, M., Ceburnis, D., Dupuy, R., and O'Dowd, C.: Nanoparticles in boreal forest and coastal environment: a comparison of observations and implications of the nucleation mechanism, Atmos. Chem. Phys., 10, 7009–7016, doi:10.5194/acp-10-7009-2010, 2010.

Lihavainen, H., Komppula, M., Kerminen, V.-M., Järvinen, H., Viisanen, Y., Lehtinen, K., Vana, M., and Kulmala, M.: Size distributions of atmospheric ions inside clouds and in cloud-free air at a remote continental site, Boreal Environ. Res., 12, 337–344, 2007.

Makkonen, R., Asmi, A., Kerminen, V.-M., Boy, M., Arneth, A., Hari, P., and Kulmala, M.: Air pollution control and decreasing new particle formation lead to strong climate warming, Atmos. Chem. Phys., 12, 1515–1524, doi:10.5194/acp-12-1515-2012, 2012.

Manninen, H. E., Petäjä, T., Asmi, E., Riipinen, I., Nieminen, T., Mikkilä, J., Horrak, U., Mirme, A., Mirme, S., and Laakso, L.: Long-term field measurements of charged and neutral clusters using Neutral cluster and Air Ion Spectrometer (NAIS), Boreal Environ. Res., 14, 591–605, 2009.

Manninen, H. E., Nieminen, T., Asmi, E., Gagné, S., Häkkinen, S., Lehtipalo, K., Aalto, P., Vana, M., Mirme, A., Mirme, S., Hõrrak, U., Plass-Dülmer, C., Stange, G., Kiss, G., Hoffer, A., Törő, N., Moerman, M., Henzing, B., de Leeuw, G., Brinkenberg, M., Kouvarakis, G. N., Bougiatioti, A., Mihalopoulos, N., O'Dowd, C., Ceburnis, D., Arneth, A., Svenningsson, B., Swietlicki, E., Tarozzi, L., Decesari, S., Facchini, M. C., Birmili, W., Sonntag, A., Wiedensohler, A., Boulon, J., Sellegri, K., Laj, P., Gysel, M., Bukowiecki, N., Weingartner, E., Wehrle, G., Laaksonen, A., Hamed, A., Joutsensaari, J., Petäjä, T., Kerminen, V.-M., and Kulmala, M.: EUCAARI ion spectrometer measurements at 12 European sites – analysis





ACPD
14, 18355–18388, 2014

of new particle formation events, Atmos. Chem. Phys., 10, 7907–7927, doi:10.5194/acp-10-7907-2010, 2010.

Manninen, H. E., Franchin, A., Schobesberger, S., Hirsikko, A., Hakala, J., Skromulis, A., Kangasluoma, J., Ehn, M., Junninen, H., Mirme, A., Mirme, S., Sipilä, M., Petäjä, T., Worsnop, D. R., and Kulmala, M.: Characterisation of corona-generated ions used in a Neutral cluster and Air Ion Spectrometer (NAIS), Atmos. Meas. Tech., 4, 2767–2776, doi:10.5194/amt-4-2767-2011, 2011.

Merikanto, J., Spracklen, D. V., Mann, G. W., Pickering, S. J., and Carslaw, K. S.: Impact of nucleation on global CCN, Atmos. Chem. Phys., 9, 8601–8616, doi:10.5194/acp-9-8601-2009, 2009.

Metzger, A., Verheggen, B., Dommen, J., Duplissy, J., Prevot, A. S. H., Weingartner, E., Riipinen, I., Kulmala, M., Spracklen, D. V., Carslaw, K. S., and Baltensperger, U.: Evidence for the role of organics in aerosol particle formation under atmospheric conditions, P. Natl. Acad. Sci. USA, 107, 6646–6651, doi:10.1073/pnas.0911330107, 2010.

Mikkonen, S., Romakkaniemi, S., Smith, J. N., Korhonen, H., Petäjä, T., Plass-Duelmer, C., Boy, M., McMurry, P. H., Lehtinen, K. E. J., Joutsensaari, J., Hamed, A., Mauldin III, R. L., Birmili, W., Spindler, G., Arnold, F., Kulmala, M., and Laaksonen, A.: A statistical proxy for sulphuric acid concentration, Atmos. Chem. Phys., 11, 11319–11334, doi:10.5194/acp-11-11319-2011, 2011.

Mirme, A., Tamm, E., Mordas, G., Vana, M., Uin, J., Mirme, S., Bernotas, T., Laakso, L., Hirsikko, A., and Kulmala, M.: A wide-range multi-channel air ion spectrometer, Boreal Environ. Res., 12, 247–264, 2007.

Mirme, S. and Mirme, A.: The mathematical principles and design of the NAIS – a spectrometer for the measurement of cluster ion and nanometer aerosol size distributions, Atmos. Meas. Tech., 6, 1061–1071, doi:10.5194/amt-6-1061-2013, 2013.

Neitola, K., Asmi, E., Komppula, M., Hyvärinen, A.-P., Raatikainen, T., Panwar, T. S., Sharma, V. P., and Lihavainen, H.: New particle formation infrequently observed in Himalayan foothills – why?, Atmos. Chem. Phys., 11, 8447–8458, doi:10.5194/acp-11-8447-2011, 2011.

Paasonen, P., Nieminen, T., Asmi, E., Manninen, H. E., Petäjä, T., Plass-Dülmer, C., Flentje, H., Birmili, W., Wiedensohler, A., Hõrrak, U., Metzger, A., Hamed, A., Laaksonen, A., Facchini, M. C., Kerminen, V.-M., and Kulmala, M.: On the roles of sulphuric acid and low-





ACPD
14, 18355–18388, 2014

volatility organic vapours in the initial steps of atmospheric new particle formation, Atmos. Chem. Phys., 10, 11223–11242, doi:10.5194/acp-10-11223-2010, 2010.
Petäjä, T., Mauldin, III, R. L., Kosciuch, E., McGrath, J., Nieminen, T., Paasonen, P., Boy, M., Adamov, A., Kotiaho, T., and Kulmala, M.: Sulfuric acid and OH concentrations in a boreal forest site, Atmos. Chem. Phys., 9, 7435–7448, doi:10.5194/acp-9-7435-2009, 2009.
Rose, C., Boulon, J., Hervo, M., Holmgren, H., Asmi, E., Ramonet, M., Laj, P., and Sellegri, K.: Long-term observations of cluster ion concentration, sources and sinks in clear sky conditions at the high-altitude site of the Puy de Dôme, France, Atmos. Chem. Phys., 13, 11573–11594, doi:10.5194/acp-13-11573-2013, 2013.
Spracklen, D. V., Carslaw, K. S., Kulmala, M., Kerminen, V.-M., Sihto, S.-L., Riipinen, I., Merikanto, J., Mann, G. W., Chipperfield, M. P., and Wiedensohler, A.: Contribution of particle formation to global cloud condensation nuclei concentrations, Geophys. Res. Lett., 35, doi:10.1029/2007GL033038, 2008.
Tammet, H. and Kulmala, M.: Simulation tool for atmospheric aerosol nucleation bursts, J. Aerosol Sci., 36, 173–196, doi:10.1016/j.jaerosci.2004.08.004, 2005.
Vanhanen, J., Mikkilä, J., Lehtipalo, K., Sipilä, M., Manninen, H. E., Siivola, E., Petäjä, T., and Kulmala, M.: Particle Size Magnifier for nano-CN detection, Aerosol Sci. Tech., 45, 533–542, doi:10.1080/02786826.2010.547889, 2011.
Venzac, H., Sellegri, K., and Laj, P.: Nucleation events detected at the high altitude site of the Puy de Dôme Research Station, France, Boreal Environ. Res., 12, 345–359, 2007.
Venzac, H., Sellegri, K., Laj, P., Villani, P., Bonasoni, P., Marinoni, A., Cristofanelli, P., Calzolari, F., Fuzzi, S., and Decesari, S.: High frequency new particle formation in the Himalayas, P. Natl. Acad. Sci. USA, 105, 15666–15671, 2008.
Venzac, H., Sellegri, K., Villani, P., Picard, D., and Laj, P.: Seasonal variation of aerosol size distributions in the free troposphere and residual layer at the puy de Dôme station, France, Atmos. Chem. Phys., 9, 1465–1478, doi:10.5194/acp-9-1465-2009, 2009.
Wang, J. and Wexler, A. S.: Adsorption of organic molecules may explain growth of newly nucleated clusters and new particle formation, Geophys. Res. Lett., doi:10.1002/grl.50455, 2013.
Wimmer, D., Lehtipalo, K., Franchin, A., Kangasluoma, J., Kreissl, F., Kürten, A., Kupc, A., Metzger, A., Mikkilä, J., Petäjä, T., Riccobono, F., Vanhanen, J., Kulmala, M., and Curtius, J.: Performance of diethylene glycol-based particle counters in the sub-3 nm size range, Atmos. Meas. Tech., 6, 1793–1804, doi:10.5194/amt-6-1793-2013, 2013.





ACPD
14, 18355–18388, 2014

**Table 1.** Summary of the particle formation event characteristics. $GR_{1.5–3}$ and $GR_{3–5}$ are the particle growth rates in 1.5–3 and 3–5 nm size ranges respectively, $J_{1.5}^{ion}$ and $J_3^{ion}$ are ion formation rates at 1.5 and 3 nm and $J_{1.5}^{tot}$ and $J_3^{tot}$ are the corresponding total particle formation rates during the event. Instruments used for the calculation of each parameter are specified in the second raw; for the NAIS also the mode used for the measurements is given. February 2012, Puy de Dôme.

| Date | $GR_{1.5–3}$ ($nm\,h^{-1}$) NAIS Ion | $GR_{3–5}$ ($nm\,h^{-1}$) NAIS Ion | $J_{1.5}^{+}$ ($cm^{-3}\,s^{-1}$) NAIS Ion | $J_{1.5}^{-}$ ($cm^{-3}\,s^{-1}$) NAIS Ion | $J_3^{+}$ ($cm^{-3}\,s^{-1}$) NAIS Ion | $J_3^{-}$ ($cm^{-3}\,s^{-1}$) NAIS Ion | $J_{1.5}^{tot}$ ($cm^{-3}\,s^{-1}$) PSM | $J_3^{tot}$ ($cm^{-3}\,s^{-1}$) NAIS Particle |
|---|---|---|---|---|---|---|---|---|
| 10 Feb | 1.65 | 8.45 | 0.084 ± 0.057 | 0.025 ± 0.033 | 0.049 ± 0.044 | 0.062 ± 0.050 | 2.87 ± 3.71 | 1.38 ± 0.91 |
| 11 Feb | 1.93 | 3.58 | – | 0.010 ± 0.030 | – | 0.013 ± 0.009 | 0.58 ± 0.64 | 0.34 ± 0.23 |
| 12 Feb | 14.36 | 15.57 | 0.468 ± 0.083 | 0.311 ± 0.100 | 0.139 ± 0.071 | 0.245 ± 0.147 | 18.24 ± 10.11 | 2.20 ± 0.94 |
| 28 Feb | 1.90 | – | 0.183 ± 0.067 | 0.022 ± 0.027 | – | – | 0.42 ± 0.28 | – |
| 29 Feb | 10.45 | 5.06 | 0.686 ± 0.148 | 0.132 ± 0.070 | 0.011 ± 0.011 | 0.011 ± 0.012 | 4.32 ± 2.84 | 0.60 ± 0.58 |





ACPD
14, 18355–18388, 2014

**Table 2.** Cluster concentrations for each sub-period. Median, 25th and 75th percentiles of charged cluster concentration ($N_i$), total cluster concentration ($N_{tot}$) and neutral cluster concentration ($N_n$) during the different periods. The indices day refer to values calculated over the whole day whereas the indices nucl refer to values calculated during the time period 10:30–14:00 LT. Indication < LDL refers to concentrations below the lower detection limit (500 $cm^{-3}$) that was set for the total cluster concentration measured by the PSM; corresponding neutral cluster concentrations which are negative are not reported. The occurrence of NPF during the sub-periods is shown in table. February 2012, Puy de Dôme.

| | Period 1, NPF | | | Period 2, No NPF | | | Period 3, NPF | | |
|---|---|---|---|---|---|---|---|---|---|
| | Med. | 25th perc. | 75th perc. | Med. | 25th perc. | 75th perc. | Med. | 25th perc. | 75th perc. |
| $N_{i_day}$ ($cm^{-3}$) | 275.0 | 187.6 | 391.9 | 651.5 | 563.3 | 690.0 | 752.3 | 681.3 | 802.8 |
| $N_{i_nucl}$ ($cm^{-3}$) | 473.1 | 392.8 | 533.2 | 656.1 | 594.1 | 694.5 | 714.8 | 657.2 | 757.3 |
| $N_{tot_nucl}$ ($cm^{-3}$) | 2049.1 | **821.9** | 7265.1 | < LDL | < LDL | < LDL | 921.4 | 715.8 | 1354.8 |
| $N_{n_nucl}$ ($cm^{-3}$) | 2022.9 | **453.7** | 6765.0 | – | – | – | **281.4** | **7.4** | 854.0 |





ACPD
14, 18355–18388, 2014

**Table 3.** Summary of the mean values of several atmospheric parameters for each sub-period. The occurrence of NPF during the sub-periods is shown in table. February 2012, Puy de Dôme.

| | Period 1, NPF | Period 2, No NPF | Period 3, NPF |
|---|---|---|---|
| $T$ (°C) | −14.24 | −1.40 | 4.96 |
| RH (%) | 90.80 | 29.32 | 51.8 |
| BC (ng m$^{-3}$) | 687.53 | 87.83 | No data |
| CS (s$^{-1}$) | $1.36 \times 10^{-2}$ | $1.60 \times 10^{-3}$ | $2.40 \times 10^{-3}$ |
| $H_2SO_4$ (molec cm$^{-3}$) | $6.98 \times 10^{6}$ | $68.78 \times 10^{6}$ | $8.59 \times 10^{6}$ |





ACPD
14, 18355–18388, 2014

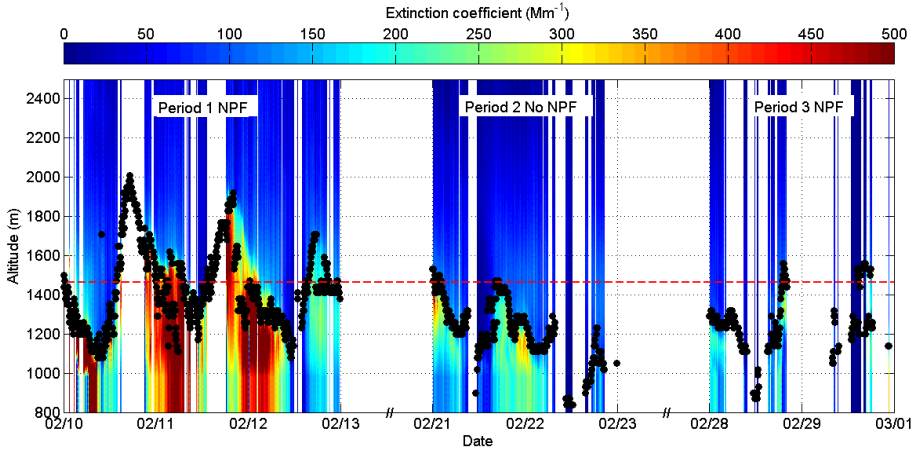


**Figure 1.** Boundary layer height determination from LIDAR measurements. In the present study, boundary layer (BL) height (black dots) is assumed to be equal to the aerosol mixing layer height and was calculating using the WCT method. Red dashed line represents the altitude of the station (1465 m a.s.l.). The presence of high altitude clouds or frost on the instrument avoids both the extinction coefficient and the BL height calculations. However, when clouds are detected at the altitude of the station, the values of the extinction calculation remain unreliable but a correct estimation of the BL height is allowed. The occurrence of NPF during the sub-periods defined in Sect. 3.2 is indicated at the top of the figure. February 2012, Puy de Dôme.





ACPD
14, 18355–18388, 2014

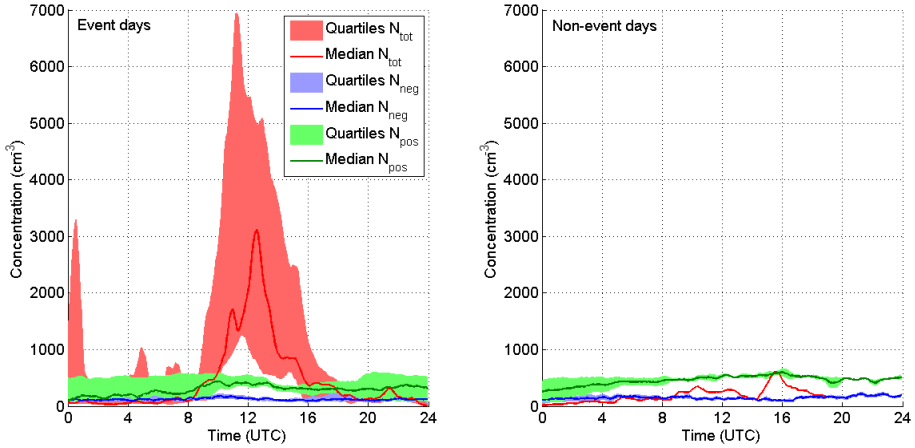


**Figure 2.** Median diurnal variation of positive ($N_{pos}$), negative ($N_{neg}$) and total ($N_{tot}$) cluster concentrations (1 to 2.5 nm mobility diameter) on new particle formation event days (left panel) and on non-event days (right panel). Lower and upper limits of the shading areas represent the first and the third quartile of the corresponding concentration. On non-event days, the lack in total cluster concentration measurement is due to an instrument failure. February 2012, Puy de Dôme.





ACPD
14, 18355–18388, 2014

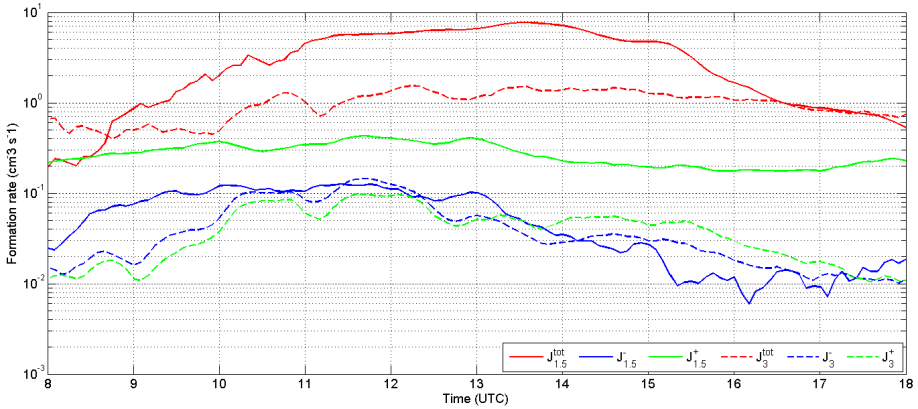


**Figure 3.** Average variation of the formation rates of 1.5 and 3.0 nm particles and ions during day time. February 2012, Puy de Dôme.





ACPD
14, 18355–18388, 2014

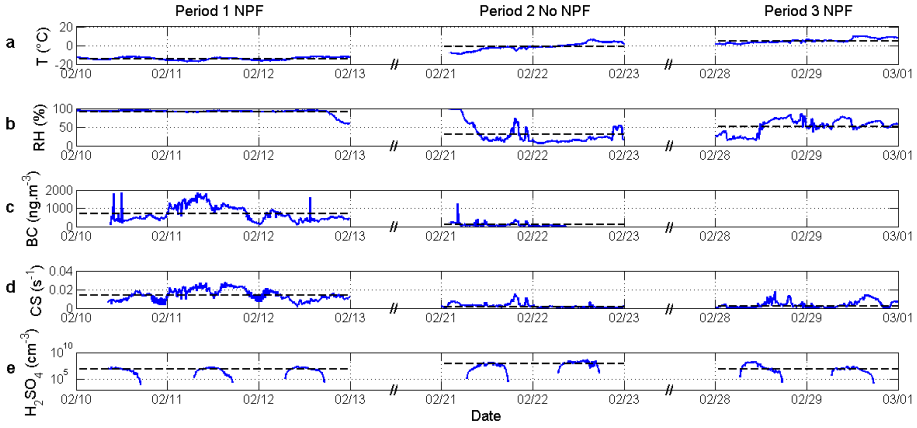


**Figure 4.** Overview of atmospheric parameters during the studied period. Black dashed lines represent the mean value of each parameter during the three sub-periods. The occurrence of NPF during the sub-periods is indicated at the top of the figure. February 2012, Puy de Dôme.





ACPD
14, 18355–18388, 2014

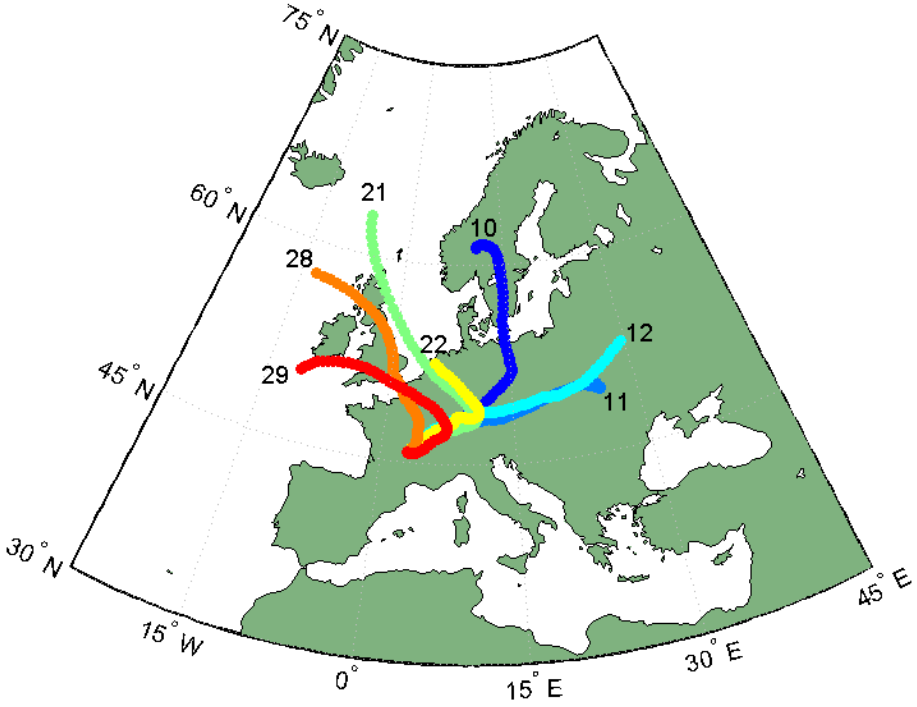


**Figure 5.** Three-days back trajectories of air masses reaching the Puy de Dôme at 12:00 UTC. Days are indicated on the map closed to the corresponding trajectories. February 2012, Puy de Dôme.





ACPD
14, 18355–18388, 2014

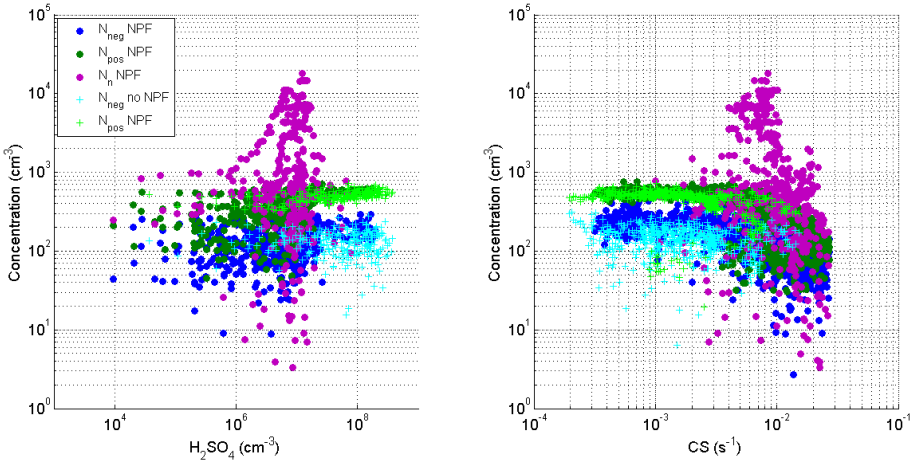


**Figure 6.** Nanoparticle concentrations as a function of potential nucleation source and sink. Positive ($N_{pos}$), negative ($N_{neg}$) and neutral cluster ($N_n$) concentrations as a function of **(a)** sulphuric acid concentration and **(b)** condensation sink are reported separately, for NPF event and non-event days. Neutral cluster concentrations which are negative on non-event days are not shown on the figure. February 2012, Puy de Dôme.





ACPD
14, 18355–18388, 2014